Letter

Probing the long-range structure of the T_{cc}^+ with the strong and electromagnetic decays

Lu Meng,[1] Guang-Juan Wang,[2] Bo Wang,[3,4,*] and Shi-Lin Zhu[5,†]

[1]*Ruhr-Universität Bochum, Fakultät für Physik und Astronomie, Institut für Theoretische Physik II, D-44780 Bochum, Germany*

[2]*Advanced Science Research Center, Japan Atomic Energy Agency, Tokai, Ibaraki 319-1195, Japan*

[3]*School of Physical Science and Technology, Hebei University, Baoding 071002, China*

[4]*Key Laboratory of High-precision Computation and Application of Quantum Field Theory of Hebei Province, Baoding 071002, China*

[5]*School of Physics and Center of High Energy Physics, Peking University, Beijing 100871, China*

(Received 16 August 2021; accepted 8 September 2021; published 28 September 2021)

Very recently, the LHCb Collaboration reported the doubly charmed tetraquark state T_{cc}^+ below the $D^{*+}D^0$ threshold about 273 keV. As a very near-threshold state, its long-distance structure is very important. In the molecular scheme, we relate the coupling constants of T_{cc}^+ with $D^{*0}D^+$ and $D^{*+}D^0$ to its binding energy and mixing angle of two components with a coupled-channel effective field theory. With the coupling constants, we investigate the kinetically allowed strong decays $T_{cc}^+ \to D^0D^0\pi^+$, $T_{cc}^+ \to D^+D^0\pi^0$ and radiative decays $D^+D^0\gamma$. Our results show that the decay width of $T_{cc}^+ \to D^0D^0\pi^+$ is the largest one, which is just the experimental observation channel. Our theoretical total strong and radiative widths are in favor of the T_{cc}^+ as a $|D^{*+}D^0\rangle$ dominated bound state. The total strong and radiative width in the single channel limit and isospin singlet limit are given as $59.7^{+4.6}_{-4.4}$ keV and $46.7^{+2.7}_{-2.9}$ keV, respectively. Our calculation is cutoff-independent and without prior isospin assignment. The absolute partial widths and ratios of the different decay channels can be used to test the structure of T_{cc}^+ state when the updated experimental results are available.

DOI: 10.1103/PhysRevD.104.L051502

I. INTRODUCTION

Very recently, the LHCb Collaboration reported the first doubly charmed tetraquark state T_{cc}^+ in the prompt production of the pp collision with a signal significance over 10σ [1]. Its mass with respect to the $D^{*+}D^0$ threshold and width are

$$\delta m = -273 \pm 61 \pm 5^{+11}_{-14}\ \text{keV},$$
$$\Gamma = 410 \pm 165 \pm 43^{+18}_{-38}\ \text{keV}. \quad (1)$$

In the fitting, the quantum number $J^P = 1^+$ is assumed. The significance for $\delta m < 0$ is 4.3σ. The LHCb Collaboration also released a decay analysis, in which the unitarized Breit-Wigner profile was used [2].[1] The mass with respect to the $D^{*+}D^0$ threshold and width read,

$$\delta m^U = -361 \pm 40\ \text{keV}, \qquad \Gamma^U = 47.8 \pm 1.9\ \text{keV}. \quad (2)$$

The observation of T_{cc}^+ is a great breakthrough for the hadron physics. It is the second doubly charmed hadron that has been observed in experiments for now. What is more interesting, it is manifestly an exotic hadron composed of four (anti)quarks.

In fact, the doubly heavy tetraquark states are anticipated and debated for 40 years [5–20]. In 2017, the first doubly charmed baryon Ξ_{cc}^{++} was observed by the LHCb Collaboration [21], which incited a new round of heated discussions on the doubly heavy tetraquark states [22–39]. An extensive review of the T_{cc} system can be found in Ref. [40]. From the theoretical perspective, a well-known fascinating feature of the compact doubly heavy tetraquark states is that they might locate below the two-meson

*Corresponding author.
wangbo@hbu.edu.cn
†Corresponding author.
zhusl@pku.edu.cn

[1]To some extent, our results agree with analysis in Ref. [2]. We should stress that the analysis was released after our work. Our calculation only based on the information in Refs. [3,4] and was independent of the Ref. [2].

thresholds and then become very narrow. The underlying reason is the possible heavy-antiquark-heavy-diquark symmetry. The doubly heavy diquark in color anti-triplet could be relatively compact, and it is an analog of the antiquark. The mass of doubly heavy compact tetraquark is constrained by its singly heavy partner in the heavy-antiquark-heavy-diquark symmetry (e.g., see [23,24,41] for details). The above analyses were well accepted for doubly bottom systems due to large bottom quark mass. However, there was no agreement for doubly charmed systems before the observation of T_{cc}^+ state.

Apart from the compact tetraquark scheme, there is another motivation to investigate the doubly heavy tetraquark states in the hadronic molecule scheme, which might not be as popular as the former one but has the equal significance. In the molecular scheme, the one-pion-exchange interaction of $\bar{D}^*D/\bar{D}D^*$ system with the quantum numbers of $I(J^{PC}) = 0(1^{++})$ [corresponding to $X(3872)$] and that of the D^*D system with $I(J^P) = 0(1^+)$ are exactly the same in the isospin symmetry limit [42–44]. The doubly charmed analog of $X(3872)$ is therefore expected [42–44]. In Ref. [44], the authors obtained a D^*D bound state with quantum numbers $I(J^P) = 0(1^+)$, in which the long-range one-pion-exchange as well as the short- and mid-range interactions by exchanging η, ρ, ω and σ mesons were included. The theoretical binding energy and root-mean-square radius are 470 keV and 4.46 fm, respectively. The predictions using the one-boson-exchange model agree very well with the newly experimental results [1]. Similar results were also obtained in chiral effective field theory [45]. After the observation of T_{cc}^+, the isospin violating effect was considered in the one-boson-exchange model [46]. The T_{cc}^+ was interpreted as a bound state composed of two channels, $\cos\theta|D^{*+}D^0\rangle + \sin\theta|D^{*0}D^+\rangle$ with $\theta \approx \pm 30.08°$. In this work, we will see the newly observed T_{cc}^+ tetraquark state does have many similarities with the $X(3872)$.

The T_{cc}^+ state is only about 300 keV below the $D^{*+}D^0$ threshold. If the T_{cc}^+ is interpreted as the bound state of $D^{*+}D^0$ in a single channel formalism, a natural consequence of such a small binding energy is the low-energy universality similar to the $X(3872)$ state [47,48]. The low-energy observables for T_{cc}^+ or $X(3872)$ are insensitive to the details of the interactions. Thus, the long-range feature of such systems only depends on the scattering length or binding energy. If the higher $D^{*0}D^+$ channel was taken into consideration in a coupled-channel formalism, the considerable isospin violation effect is expected due to the sensitivity of the structure to the threshold differences for such a very near-threshold bound state. In this work, we aim to uncover the structure of the T_{cc}^+ through its long-distance dynamics, the strong and radiative decays. We will resort to an effective field theory satisfying the renormalization group invariance. The coupling constants of T_{cc}^+ with $D^{*+}D^0$ and $D^{*0}D^+$ will be related to the binding energy and mixing angle of the two components. The strong and radiative decay widths can provide important information about its structure.

This work is organized as follows. In Sec. II, we use a coupled-channel effective field theory to relate the coupling constants to the binding energy and mixing angle of the two components. In Sec. III, we calculate the strong and radiation decays for the T_{cc}^+ states and provide some insights into its structure. In Sec. IV, we give a brief summary.

II. COUPLING CONSTANTS AND WAVE FUNCTIONS

In the molecular scheme, the two closest thresholds are $D^{*+}D^0$ and $D^{*0}D^+$, which are located above the T_{cc}^+ about 0.3 MeV and 1.7 MeV, respectively. The components of the bound state will be sensitive to the threshold mass gaps and the large isospin violation effect is expected [43]. Therefore, we will introduce the coupled-channel effect dynamically rather than presuming a prior isospin assignment. The two related channels are noted as $|1\rangle \equiv |D^{*+}D^0\rangle$ and $|2\rangle \equiv |D^{*0}D^+\rangle$. We adopt a coupled-channel effective field theory proposed by Cohen *et al.* [49], which is well used in hadron physics [50–52] and nuclear physics [53]. We will see that in this effective field theory, the cutoff-dependence can be eliminated exactly, which makes it renormalization group invariant.

For the effective field theory, we introduce the leading order interaction

$$V(\boldsymbol{p},\boldsymbol{p}') = \begin{bmatrix} v_{11} & v_{12} \\ v_{12} & v_{22} \end{bmatrix} \Theta(\Lambda - p)\Theta(\Lambda - p'), \quad (3)$$

where v_{ij} are energy-independent parameters. The step function Θ serves as a hard regulator and Λ is the cutoff parameter. For such a separable interaction, the $T(\boldsymbol{p},\boldsymbol{p}')$ has the similar separable form with $T(\boldsymbol{p},\boldsymbol{p}') = t\Theta(\Lambda - p)\Theta(\Lambda - p')$, where t is the matrix of elements t_{ij}. The coupled-channel Lippmann-Schwinger equations (LSEs) can be reduced to a set of algebraic equations,

$$t = v + vGt \Rightarrow t = (1 - vG)^{-1}v, \quad (4)$$

where $G = \mathrm{diag}\{G_1, G_2\}$. The G_i reads

$$G_i(E) = \int^{\Lambda} \frac{d^3\boldsymbol{q}}{(2\pi)^3} \frac{1}{E - E_{i,q} + i\epsilon},$$
$$E_{i,q} = \delta_i + \frac{q^2}{2\mu}, \quad (5)$$

where μ is the reduced mass of di-mesons. In this work, we can neglect the tiny differences of the reduced masses in the two channels. The δ_i is the mass difference with

respect to $D^{*+}D^0$ threshold. Then we have $\delta_1 = 0$ and $\delta = \delta_2 \equiv m_{D^{*0}} + m_{D^+} - (m_{D^{*+}} + m_{D^0})$. For a bound state with $E < 0$, the explicit expression of $G_i(E)$ reads

$$G_i(E) = \frac{\mu}{\pi^2}\left[-\Lambda + k_i \arctan\frac{\Lambda}{k_i}\right] \approx \frac{\mu}{2\pi}\left[-\frac{2}{\pi}\Lambda + k_i\right], \quad (6)$$

where $k_1 \equiv \sqrt{-2\mu E}$ and $k_2 \equiv \sqrt{-2\mu(E-\delta)}$. The approximation in Eq. (6) is a consequence of $|k_i| \ll \Lambda$. It is straightforward to obtain the solution of the LSEs,

$$t = \frac{1}{D}\begin{bmatrix} b_{11}b_{12}^2(1 - b_{22}k_2) & b_{11}b_{12}b_{22} \\ b_{11}b_{12}b_{22} & b_{12}^2 b_{22}(1 - b_{11}k_1) \end{bmatrix}, \quad (7)$$

where $D = \frac{\mu}{2\pi}[b_{12}^2(b_{11}k_1 - 1)(b_{22}k_2 - 1) - b_{11}b_{22}]$ and the b_{ij} are introduced as

$$\begin{cases} \frac{1}{b_{11}} & = \frac{2\pi}{\mu}\left(\frac{v_{22}}{v_{11}v_{22} - v_{12}^2} - G_1\right) + k_1 \\ \frac{1}{b_{22}} & = \frac{2\pi}{\mu}\left(\frac{v_{11}}{v_{11}v_{22} - v_{12}^2} - G_2\right) + k_2\,. \\ \frac{1}{b_{12}} & = \frac{2\pi}{\mu}\frac{v_{12}}{v_{11}v_{22} - v_{12}^2} \end{cases} \quad (8)$$

One can see that the cutoff dependence of G_i in Eq. (8) can be absorbed by renormalizing v_{ij}. In this way, the cutoff dependence can be eliminated exactly. The similar results were derived in Refs. [49,50].

The bound state T_{cc}^+ corresponds to a pole in the real axial of the complex energy plane. The residuals of the t matrix can be related to the coupling constants of the bound state with the corresponding dimeson channels [54,55]. In our normalization convention, we have

$$\lim_{E\to E_0}(E - E_0)t_{ij} = \lim_{E\to E_0}\left[\frac{d(t_{ij})^{-1}}{dE}\right]^{-1} = \frac{1}{8M_T^2\mu}g_i g_j \quad (9)$$

where E_0 is the pole corresponding to the T_{cc}^+ state. M_T is the mass of T_{cc}^+ and g_i is its coupling constant to the two $\bar{D}D^*$ channels. A straightforward derivation gives a very simple expression for $\lim_{E\to E_0}(E - E_0)t$, which reads

$$\frac{2\pi}{\mu^2}\begin{bmatrix} \kappa_1 \cos^2\theta & \sqrt{\kappa_1\kappa_2}\sin\theta\cos\theta \\ \sqrt{\kappa_1\kappa_2}\sin\theta\cos\theta & \kappa_2 \sin^2\theta \end{bmatrix}, \quad (10)$$

where κ_i and θ are defined as

$$\kappa_i \equiv \lim_{E\to E_0} k_i, \qquad \tan^2\theta \equiv \frac{b_{22}\kappa_1(b_{11}\kappa_1 - 1)}{b_{11}\kappa_2(b_{22}\kappa_2 - 1)}. \quad (11)$$

We will see that θ is actually the mixing angle of the two channels in the T_{cc}^+ state. The coupling constants read

$$g_1 = \frac{4M_T\sqrt{\pi\kappa_1}}{\sqrt{\mu}}\cos\theta, \qquad g_2 = \frac{4M_T\sqrt{\pi\kappa_2}}{\sqrt{\mu}}\sin\theta. \quad (12)$$

We want to emphasize that our results are more general than those in Refs. [54,55], in which $v_{11} = v_{12} = v_{22} = v$ is assumed.

In principle, the coupling constants obtained from the residuals of the T-matrix can be related to the wave functions for the bound states [50,54,56,57]. In our interaction the Schrödinger equation reads,

$$(\hat{H}_0 + \hat{V})|\psi\rangle = E_0|\psi\rangle, \qquad \hat{V} = \sum_{i,j}\frac{1}{(2\pi)^3}v_{ij}|i\rangle\langle j|. \quad (13)$$

The solution of the coupled-channel equation can be obtained by the combination of the single-channel wave functions,

$$\langle \boldsymbol{p}|\psi\rangle = c_1\phi_1(p)|1\rangle + c_2\phi_2(p)|2\rangle, \quad (14)$$

$$\phi_i(p) = \xi_i\frac{\Theta(\Lambda - p)}{E_0 - \frac{p^2}{2\mu} - \delta_i}, \qquad \xi_i^2 \approx \frac{\kappa_i}{4\pi^2\mu^2}, \quad (15)$$

where ξ_i is the normalization constant. c_i is the coefficient of two components and satisfies $c_1^2 + c_2^2 = 1$. For the T-matrix, one can take the approximation near the bound state pole [57],

$$T_{ij}(\boldsymbol{p}, \boldsymbol{p}') \approx (2\pi)^3\frac{\langle \boldsymbol{p}, i|\hat{V}|\psi\rangle\langle\psi|\hat{V}|\boldsymbol{p}', j\rangle}{E - E_0}, \quad (16)$$

where $\langle \boldsymbol{p}, i|\hat{V}|\psi\rangle$ can be substituted by

$$\begin{aligned}\langle \boldsymbol{p}, i|\hat{V}|\psi\rangle &= \langle p, i|\hat{H} - \hat{H}_0|\psi\rangle = \left(E_0 - \frac{p^2}{2\mu} - \delta_i\right)\langle \boldsymbol{p}, i|\psi\rangle \\ &= c_i\xi_i\Theta(\Lambda - p). \end{aligned} \quad (17)$$

Therefore, we obtain the element of T-matrix,

$$t_{ij} \approx (2\pi)^3\frac{c_i c_j \xi_i \xi_j}{E - E_0}. \quad (18)$$

Comparing the above expression with Eq. (10), one can obtain the meaning of c_i,

$$c_1 = \cos\theta, \qquad c_2 = \sin\theta. \quad (19)$$

Thus, we proved that the θ defined in Eq. (11) is in fact the mixing angle of the $|1\rangle$ and $|2\rangle$ components.

One can see the coupling constants in Eq. (12) depend on the binding energy (in κ_i) and the mixing angle θ. In the single channel limit ($\theta = 0$), the coupling constant and the wave function only depend on the binding energy, which is the manifestation of the universality of the low energy

dynamics. In the realistic case, the long-range dynamics of T_{cc}^{+} will rely on the mixing angle. One can extract the structure information of T_{cc}^{+} by investigating its strong and radiative decays.

III. STRONG DECAY AND RADIATIVE DECAY

The strong and radiative decays of T_{cc}^{+} state are illustrated in Fig. 1. The details for the determinations of the coupling constants of $D^{*} \to D\pi(\gamma)$, the strong and radiative decay amplitudes of T_{cc}^{+}, as well as the each diagram contribution in ideal single-channel cases are given in Appendix. Here, we list some main conclusions that one can read from Appendix. The results show that the Fig. 1(s_b) and (r_b) are the dominant diagrams contributing to the strong and radiative decays, respectively, which are almost 4 times larger than the contributions from other diagrams. For the strong decays, we use (s_b) to represent two diagrams considering the exchange of two identical D^0 final state. The amplitude of diagram (s_b) is amplified by an extra isospin factor $\sqrt{2}$ in the $D^{*+}D^0\pi^+$ vertex and considerable interference effect of two diagrams. For the radiative decays, the amplitude of (r_b) is much larger than that of (r_a), because the leading amplitudes for M1 radiative transition $D^{*0,+} \to D^{0,+}\gamma$ are roughly proportional to the electric charges of the light quarks in the heavy quark limit. In addition, the strong decay width arising from (s_b) is also much larger than the radiative one from (r_b).

However, the realistic situation is the strong and radiative decay widths depend on the binding energy of T_{cc}^{+} as well as the mixing angle of two components [see Eq. (12)]. We list three special angles and their corresponding states as follows,

$$|T_{cc}^{+}\rangle = \cos\theta|D^{*+}D^{0}, \phi_1\rangle + \sin\theta|D^{*0}D^{+}, \phi_2\rangle, \tag{20}$$

$$\theta = \begin{cases} 0 & \text{pure} D^{*+}D^{0} \\ \frac{\pi}{4} & I = 1, I_3 = 0 \\ -\frac{\pi}{4} & I = 0, I_3 = 0 \end{cases}. \tag{21}$$

Either the absolute value or the relative ratios of the partial decay widths, embed the important information about the structure of the T_{cc}^{+} state. We present the strong and radiative decay widths in Figs. 2 and 3. We can obtain several nontrivial conclusions from them.

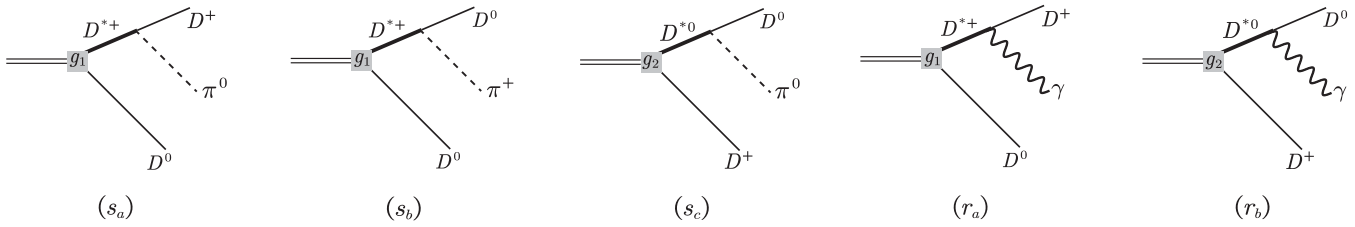

FIG. 1. The Feynman diagrams for strong and radiative decays of the T_{cc}^{+} state, where the vertices marked by g_1 and g_2 denote the coupling strengths of T_{cc}^{+} to the channels $|1\rangle$ and $|2\rangle$, respectively.

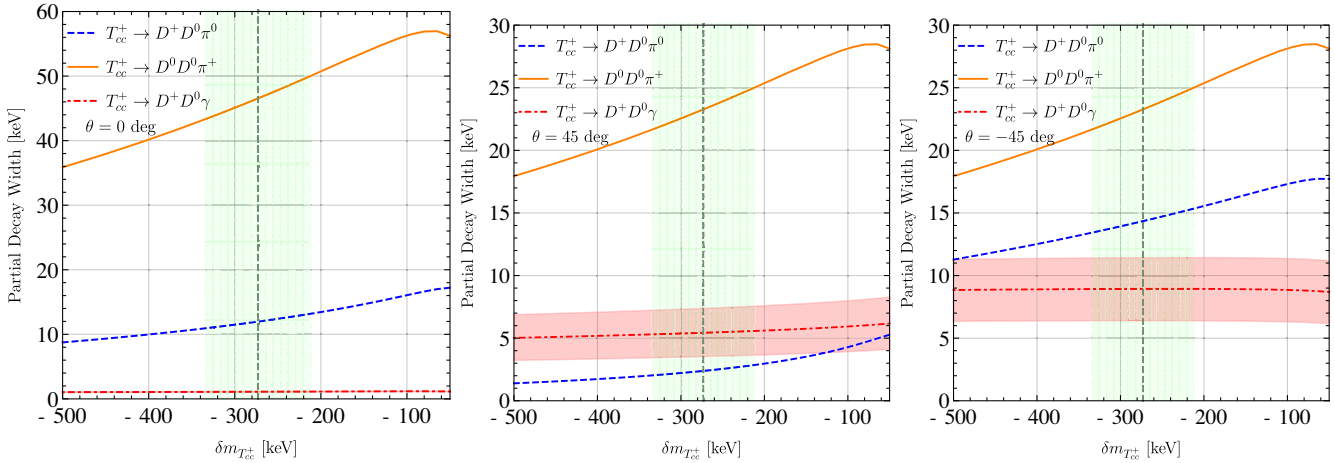

FIG. 2. The dependence of the strong and radiative decay widths on binding energy for the T_{cc}^{+} state. Three subfigures from the left to right show the decay widths of single channel $(D^{*+}D^{0})$, $I = 1$ (isospin triplet) and $I = 0$ (isospin singlet) configurations, respectively. The green band represents the uncertainty of the T_{cc}^{+} mass. The vertical dashed line is the central value of the binding energy. For the radiative decay, the red shadow represents the uncertainties arising from the unfixed D^{*0} width (40–80 keV is used).

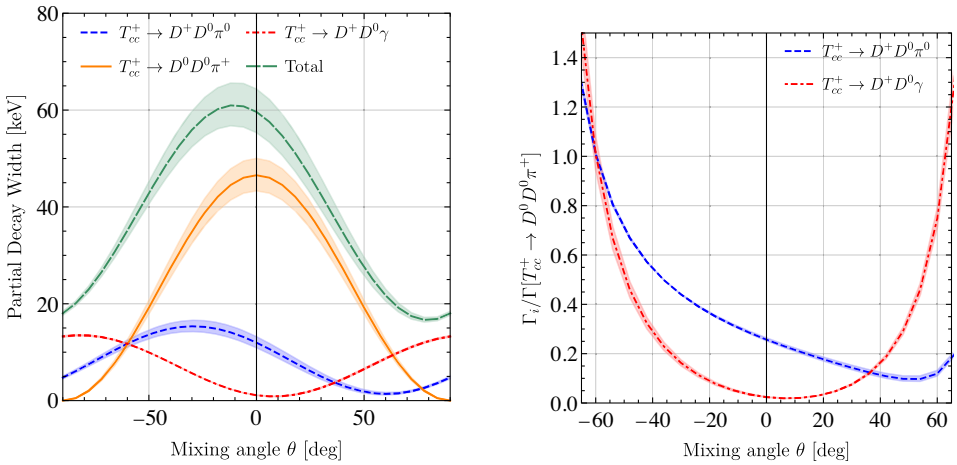

FIG. 3. The dependence on the mixing angle for the T_{cc}^+ strong and radiative decay. The left and the right subfigure show the absolute values and relative ratios of the decay widths. The colored shadow represents the uncertainties stemming from the T_{cc}^+ mass in Eq. (1).

The first and the foremost conclusion is that the dominant decay mode of the T_{cc}^+ is $D^0D^0\pi^+$, which is just its observation channel in experiments. In Fig. 2, we present the partial decay widths with the mixing angle $\theta = 0$, $\pi/4$ and $-\pi/4$, which correspond to the single channel $D^{*+}D^0$, $I = 1$ and $I = 0$ cases, respectively. In these three configurations, the dominant decay mode is $T_{cc}^+ \to D^0D^0\pi^+$. In the left subfigure of Fig. 3, we show the dependence of the decay widths on the mixing angle. One can see that the $T_{cc}^+ \to D^0D^0\pi^+$ is dominant in most mixing structures. The exception only appears when the bound state is almost pure $D^{*0}D^+$ bound state ($|\theta| \sim \pi/2$). But it is less likely that a bound state (below two thresholds) in two-channel interaction model contains more higher channel component. Thus, in the molecular scheme, it is easy to understand why the T_{cc}^+ is firstly observed in the $D^0D^0\pi^+$ final state rather than other channels.

Meanwhile, the experimental decay width of T_{cc}^+ is in favor of the $|D^{*+}D^0\rangle$ dominant molecule structure. In the left subfigure of Fig. 3, the maximum of the total decay width appears at $\theta \approx 0$, because the dominant decay mode $T_{cc}^+ \to D^0D^0\pi^+$ is induced by the $D^{*+}D^0$ channel through the coupling constant g_1 proportional to $\cos\theta$. From Eq. (6), we can see the partial decay width achieves its maximum when $\theta \approx 0$, which corresponds to the single channel limit. In this limit, we obtain the total width of T_{cc}^+ from the strong and the radiative decays as

$$\text{Single-channel limit}: \Gamma_{\text{str}} + \Gamma_{\text{EM}} = 59.7^{+4.6}_{-4.4}\ \text{keV}. \quad (22)$$

This decay width is still smaller that the central value 410 keV in experiment. The difference might be resolved when the experimental resolution is improved in the future. The parameters of near-threshold resonance would be sensitive to the line shape parametrization formalism.[2] The total widths from the strong and radiative decays for the isospin singlet and triplet state read,

$$\text{Isospin singlet}: \Gamma_{\text{str}} + \Gamma_{\text{EM}} = 46.7^{+2.7}_{-2.9}\ \text{keV}, \quad (23)$$

$$\text{Isospin triplet}: \Gamma_{\text{str}} + \Gamma_{\text{EM}} = 31.2^{+2.2}_{-2.4}\ \text{keV}. \quad (24)$$

The decay widths for the isospin singlet and triplet assignments are smaller than the experimental data. Therefore, one can expect that, with the improving of the measurement resolution, the decay width of T_{cc}^+ would be in accordance with a $D^{*+}D^0$-dominated bound state rather than the isospin triplet or the singlet. In other words, large isospin violation for T_{cc}^+ is supported by the present experimental results.

In the right subfigure of Fig. 3, we present the ratios of different partial decay widths. One can see that the ratio of $\Gamma[T_{cc}^+ \to D^+D^0\pi^0]/\Gamma[T_{cc}^+ \to D^0D^0\pi^+]$ is sensitive to the mixing angle when the angle is in the range of $(-\pi/4, \pi/4)$. When the bound state is approaching to the isospin singlet (triplet), the ratio will increase (decrease). Meanwhile, if the T_{cc}^+ is dominated by the $D^{*+}D^0$ component, the radiative decay will be extremely suppressed, because the contribution from the most important diagram (r_b) is suppressed by the $\sin^2\theta$ in the coupling constants.

IV. SUMMARY

In this work, we study the strong and radiative decays of the newly reported doubly charmed T_{cc}^+ state. The T_{cc}^+ state is very close to the threshold D^*D. It seems to be a sibling

[2]The analysis from LHCb Collaboration after this work with unitarized Breit-Wigner formalism did decrease the width [2].

of $X(3872)$ in the double-charm systems. Its long-range structure is very important due to the quite small binding energy. In the molecular scheme, we investigate the kinetics-allowed strong decays $T_{cc}^+ \to D^0D^0\pi^+$, $T_{cc}^+ \to D^+D^0\pi^0$ and radiative decays $D^+D^0\gamma$, which are sensitive to the long-range structure of T_{cc}^+.

In our calculations, we include the $D^{*+}D^0$ and $D^{*0}D^+$ as two channels rather than presuming prior isospin assignment. We adopt a well-used coupled-channel effective field theory, which is cutoff-independent and satisfies the renormalization group invariance. We extract the coupling constants of T_{cc}^+ to $D^{*+}D^0$ and $D^{*0}D^+$ channels from the residuals of the T-matrix. We relate the coupling constants to the wave functions in the Schrödinger equation. Our results show the coupling constants depend on both the binding energy and the mixing angle of the two channels. With the coupling constants and the strong and radiation vertices of D^* mesons from experiments, we obtain the strong and radiative decay widths of T_{cc}^+. Our numerical results show that the decay width of $T_{cc}^+ \to D^0D^0\pi^+$ is the largest one, which is consistent with the experimental observation. We also find the theoretical total strong and radiative width will approach the experimental value in the single channel limit (pure $D^{*+}D^0$ component), which reads $\Gamma_{\rm str} + \Gamma_{\rm EM} = 59.7^{+4.6}_{-4.4}$ keV. Thus, we can infer that the mixing angle would be very small. If the T_{cc}^+ is the pure $D^{*+}D^0$ molecule, the radiative decay width is very tiny, which is less likely to be detected in the near future. The ratio of $\Gamma[T_{cc}^+ \to D^+D^0\pi^0]/\Gamma[T_{cc}^+ \to D^0D^0\pi^+]$ is sensitive to the mixing angle when the angle is in the range of $(-\pi/4, \pi/4)$. Therefore, it can be used to judge the proportion of D^0D^{*+} and D^+D^{*0} inside the T_{cc}^+.

Our results do not depend on the cutoff parameter. The isospin violation effect is rigorously considered in coupled-channel formalism, and all the relevant uncertainties are seriously estimated. Once the new experimental results for the decays of T_{cc}^+ are available, one can easily read out its inner structure information from Figs. 2 and 3. Unlike the $X(3872)$, there is no hidden-charm channel [e.g., $J/\psi\rho$, $J/\psi\omega$ and $\chi_{c1}(2P)$ channels for $X(3872)$] interference to T_{cc}^+, so this state can also give us a very clean platform to uncover the interaction details between a pair of charmed mesons.

After this work, the LHCb Collaboration released the analysis within the unitarized Breit-Wigner formalism [2]. One can see their results in Eq. (2) are in accordance with ours in Eqs. (22)–(24).

ACKNOWLEDGMENTS

We are grateful to the helpful discussions with Prof. Eulogio Oset and Dr. Rui Chen. We also thank Mikhail Mikhasenko for helpful discussions. This project was supported by the National Natural Science Foundation of China (Grants No. 11975033 and No. 12070131001). This project was also funded by the Deutsche Forschungsgemeinschaft (DFG, German Research Foundation, Project ID No. 196253076-TRR 110). G. J. Wang was supported by JSPS KAKENHI (No. 20F20026). B. W. was supported by the Start-up Funds for Young Talents of Hebei University (No. 521100221021).

APPENDIX: AMPLITUDE CALCULATION

We first use Fig. 1(s_a) as an example to illustrate the calculation of the strong decay. The $D^{*+} \to D^+\pi^0$ amplitude is $\mathcal{A} = g_\pi q_\pi \cdot \epsilon_{D^*}$, where ϵ_{D^*} and q_π are the polarization vector of D^* mesons and momentum of pion, respectively. The differences of g_π extracted from $D^{*+} \to D^+\pi^0$ and $D^{*+} \to D^0\pi^+$ decays are very tiny (constrained by the isospin symmetry) [58]. We take the averaged value of coupling constant $g_\pi \simeq 11.9$ as our input. Since the D^{*0} width is still unknown, we assume the isospin symmetry and use the same coupling constant as that of the D^{*+}. Finally, the amplitude of $T_{cc}^+ \to D^+D^0\pi^0$ reads

$$\mathcal{A}[T_{cc}^+ \to D^+D^0\pi^0] = \frac{g_1\epsilon_T^\mu(g_{\mu\nu} - \frac{p_{12\mu}p_{12\nu}}{m_{D^*}^2})g_\pi p_2^\nu}{p_{12}^2 - m_{D^*}^2 + im_{D^*}\Gamma_{D^*}}, \quad \text{(A1)}$$

where ϵ_T^μ represents the polarization vector of T_{cc}^+. p_{12} and p_2 stand for the momenta of the D^{*+} and π^0, respectively. Γ_{D^*} is the width of D^* meson.

We then use the Fig. 1(r_a) to illustrate the calculation of radiative decay amplitude. The radiative decay vertex of $D^* \to D\gamma$ can be parametrized as follows,

$$\mathcal{A}[D^* \to D\gamma] = g_\gamma\epsilon_{\mu\nu\alpha\beta}\epsilon_\gamma^\mu p_{D^*}^\nu p_\gamma^\alpha \epsilon_{D^*}^\beta, \quad \text{(A2)}$$

where g_γ denotes the effective coupling constant. Its value is extracted from the partial decay widths of $D^{*+,0} \to D^{+,0}\gamma$

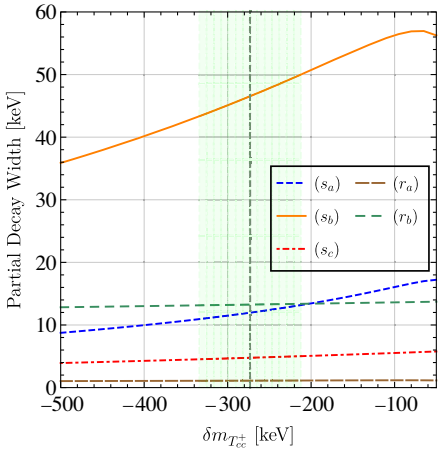

FIG. 4. The contribution to the partial widths of T_{cc}^+ from each Feynman diagram, where the interferences between diagrams with the same final states are switched off. The $\cos\theta$ and $\sin\theta$ in coupling constants of Eq. (12) are both set to be 1.

[58], respectively. For the D^{*0} meson, we take its total width as a range 40–80 keV, which covers the most of the theoretical results, e.g., [59–62]. Then the $T_{cc}^{+} \to D^{+}D^{0}\gamma$ amplitude reads

$$\mathcal{A}[T_{cc}^{+} \to D^{+}D^{0}\gamma] = \frac{g_1 \epsilon_T^{\mu}(g_{\mu\nu} - \frac{p_{12\mu}p_{12\nu}}{m_{D^*}^2}) g_\gamma \varepsilon_{\rho\sigma\alpha\nu} \epsilon_\gamma^{\rho} p_{D^*}^{\sigma} p_\gamma^{\alpha}}{p_{12}^2 - m_{D^*}^2 + i m_{D^*}\Gamma_{D^*}}. \quad \text{(A3)}$$

In order to identify the dominant diagrams, we estimate the contribution of each diagram by switching off the interference effect and replace the $\cos\theta$ and $\sin\theta$ with 1. The results in Fig. 4 show that the (s_b) and (r_b) are the dominant diagrams contributing to the strong and radiative decays, respectively, which are almost 4 times larger than the contributions from other diagrams. The strong decay width arising from (s_b) is also much larger than the radiative one from (r_b).

[1] R. Aaij *et al.* (LHCb Collaboration), arXiv:2109.01038.
[2] R. Aaij *et al.* (LHCb Collaboration), arXiv:2109.01056.
[3] I. Polyakov, Proceedings of the EPS-HEP Conference 2021: Recent LHCb Results on Exotic Meson Candidates, https://indico.desy.de/event/28202/contributions/105627/.
[4] F. Muheim, Proceedings of the EPS-HEP Conference 2021: Highlights from the LHCb Experiment, https://indico.desy.de/event/28202/contributions/102717/.
[5] J. Carlson, L. Heller, and J. A. Tjon, Phys. Rev. D **37**, 744 (1988).
[6] B. Silvestre-Brac and C. Semay, Z. Phys. C **57**, 273 (1993).
[7] C. Semay and B. Silvestre-Brac, Z. Phys. C **61**, 271 (1994).
[8] S. Pepin, F. Stancu, M. Genovese, and J. M. Richard, Phys. Lett. B **393**, 119 (1997).
[9] B. A. Gelman and S. Nussinov, Phys. Lett. B **551**, 296 (2003).
[10] J. Vijande, F. Fernandez, A. Valcarce, and B. Silvestre-Brac, Eur. Phys. J. A **19**, 383 (2004).
[11] D. Janc and M. Rosina, Few Body Syst. **35**, 175 (2004).
[12] Y. Cui, X.-L. Chen, W.-Z. Deng, and S.-L. Zhu, High Energy Phys. Nucl. Phys. **31**, 7 (2007), arXiv:hep-ph/0607226.
[13] F. S. Navarra, M. Nielsen, and S. H. Lee, Phys. Lett. B **649**, 166 (2007).
[14] J. Vijande, E. Weissman, A. Valcarce, and N. Barnea, Phys. Rev. D **76**, 094027 (2007).
[15] D. Ebert, R. N. Faustov, V. O. Galkin, and W. Lucha, Phys. Rev. D **76**, 114015 (2007).
[16] S. H. Lee and S. Yasui, Eur. Phys. J. C **64**, 283 (2009).
[17] Y. Yang, C. Deng, J. Ping, and T. Goldman, Phys. Rev. D **80**, 114023 (2009).
[18] M.-L. Du, W. Chen, X.-L. Chen, and S.-L. Zhu, Phys. Rev. D **87**, 014003 (2013).
[19] G. Q. Feng, X. H. Guo, and B. S. Zou, arXiv:1309.7813.
[20] Y. Ikeda, B. Charron, S. Aoki, T. Doi, T. Hatsuda, T. Inoue, N. Ishii, K. Murano, H. Nemura, and K. Sasaki, Phys. Lett. B **729**, 85 (2014).
[21] R. Aaij *et al.* (LHCb Collaboration), Phys. Rev. Lett. **119**, 112001 (2017).
[22] S.-Q. Luo, K. Chen, X. Liu, Y.-R. Liu, and S.-L. Zhu, Eur. Phys. J. C **77**, 709 (2017).
[23] M. Karliner and J. L. Rosner, Phys. Rev. Lett. **119**, 202001 (2017).
[24] E. J. Eichten and C. Quigg, Phys. Rev. Lett. **119**, 202002 (2017).
[25] Z.-G. Wang, Acta Phys. Pol. B **49**, 1781 (2018).
[26] G. K. C. Cheung, C. E. Thomas, J. J. Dudek, and R. G. Edwards (Hadron Spectrum Collaboration), J. High Energy Phys. 11 (2017) 033.
[27] W. Park, S. Noh, and S. H. Lee, Nucl. Phys. **A983**, 1 (2019).
[28] A. Francis, R. J. Hudspith, R. Lewis, and K. Maltman, Phys. Rev. D **99**, 054505 (2019).
[29] P. Junnarkar, N. Mathur, and M. Padmanath, Phys. Rev. D **99**, 034507 (2019).
[30] C. Deng, H. Chen, and J. Ping, Eur. Phys. J. A **56**, 9 (2020).
[31] G. Yang, J. Ping, and J. Segovia, Phys. Rev. D **101**, 014001 (2020).
[32] M.-Z. Liu, T.-W. Wu, M. Pavon Valderrama, J.-J. Xie, and L.-S. Geng, Phys. Rev. D **99**, 094018 (2019).
[33] Y. Tan, W. Lu, and J. Ping, Eur. Phys. J. Plus **135**, 716 (2020).
[34] Q.-F. Lü, D.-Y. Chen, and Y.-B. Dong, Phys. Rev. D **102**, 034012 (2020).
[35] E. Braaten, L.-P. He, and A. Mohapatra, Phys. Rev. D **103**, 016001 (2021).
[36] D. Gao, D. Jia, Y.-J. Sun, Z. Zhang, W.-N. Liu, and Q. Mei, arXiv:2007.15213.
[37] J.-B. Cheng, S.-Y. Li, Y.-R. Liu, Z.-G. Si, and T. Yao, Chin. Phys. C **45**, 043102 (2021).
[38] S. Noh, W. Park, and S. H. Lee, Phys. Rev. D **103**, 114009 (2021).
[39] R. N. Faustov, V. O. Galkin, and E. M. Savchenko, Universe **7**, 94 (2021).
[40] Y.-R. Liu, H.-X. Chen, W. Chen, X. Liu, and S.-L. Zhu, Prog. Part. Nucl. Phys. **107**, 237 (2019).
[41] T. D. Cohen and P. M. Hohler, Phys. Rev. D **74**, 094003 (2006).
[42] J. M. Dias, S. Narison, F. S. Navarra, M. Nielsen, J. M. Richard, S. Narison, and J. M. Richard, Phys. Lett. B **703**, 274 (2011).
[43] N. Li and S.-L. Zhu, Phys. Rev. D **86**, 074022 (2012).

[44] N. Li, Z.-F. Sun, X. Liu, and S.-L. Zhu, Phys. Rev. D **88**, 114008 (2013).
[45] H. Xu, B. Wang, Z.-W. Liu, and X. Liu, Phys. Rev. D **99**, 014027 (2019).
[46] R. Chen, Q. Huang, X. Liu, and S.-L. Zhu, arXiv: 2108.01911 [Phys. Rev. D (to be published)].
[47] E. Braaten and M. Kusunoki, Phys. Rev. D **69**, 074005 (2004).
[48] E. Braaten and H. W. Hammer, Phys. Rep. **428**, 259 (2006).
[49] T. D. Cohen, B. A. Gelman, and U. van Kolck, Phys. Lett. B **588**, 57 (2004).
[50] E. Braaten and M. Kusunoki, Phys. Rev. D **72**, 054022 (2005).
[51] L. Meng, B. Wang, and S.-L. Zhu, Sci. Bull. **66**, 1413 (2021).
[52] X.-K. Dong, F.-K. Guo, and B.-S. Zou, Phys. Rev. Lett. **126**, 152001 (2021).
[53] R. Higa, P. Premarathna, and G. Rupak, arXiv:2009.09324.
[54] D. Gamermann, J. Nieves, E. Oset, and E. Ruiz Arriola, Phys. Rev. D **81**, 014029 (2010).
[55] D. Gamermann and E. Oset, Phys. Rev. D **80**, 014003 (2009).
[56] F. Aceti and E. Oset, Phys. Rev. D **86**, 014012 (2012).
[57] T. Sekihara, Phys. Rev. C **95**, 025206 (2017).
[58] P. A. Zyla *et al.* (Particle Data Group Collaboration), Prog. Theor. Exp. Phys. **2020**, 083C01 (2020).
[59] D. Ebert, R. N. Faustov, and V. O. Galkin, Phys. Lett. B **537**, 241 (2002).
[60] H.-M. Choi, Phys. Rev. D **75**, 073016 (2007).
[61] D. Becirevic and B. Haas, Eur. Phys. J. C **71**, 1734 (2011).
[62] B. Wang, B. Yang, L. Meng, and S.-L. Zhu, Phys. Rev. D **100**, 016019 (2019).